2D Materials

LETTER

Heteroepitaxial growth of wafer scale highly oriented graphene using inductively coupled plasma chemical vapor deposition

Libo Gao[1,2], **Hai Xu**[2], **Linjun Li**[2], **Yang Yang**[3], **Qiang Fu**[3], **Xinhe Bao**[3] **and Kian Ping Loh**[2]

[1] National Laboratory of Solid State Microstructures, School of Physics, Collaborative Innovation Center of Advanced Microstructures, Nanjing University, Nanjing 210093, People's Republic of China
[2] Centre for Advanced 2D Materials and Department of Chemistry, National University of Singapore, Singapore 117543, Singapore
[3] State Key Laboratory of Catalysis, iChEM, Dalian Institute of Chemical Physics, Chinese Academy of Sciences, Dalian 116023, People's Republic of China

E-mail: lbgao@nju.edu.cn and chmlohkp@nus.edu.sg

RECEIVED
1 February 2016

REVISED
4 March 2016

ACCEPTED FOR PUBLICATION
14 March 2016

PUBLISHED
30 March 2016

Keywords: graphene, heteroepitaxial, CVD, grain boundary, nanocrystal

Supplementary material for this article is available online

Abstract

The chemical vapor deposition (CVD) of graphene on Cu has attracted much attention because of its industrial scalability. Herein, we report inductively coupled plasma-assisted CVD of epitaxially grown graphene on (111)-textured Cu film alloyed with a small amount of Ni, where large area high quality graphene film can be grown in less than 5 min at 800 °C, thus affording industrial scalability. The epitaxially grown graphene films on (111)-textured Cu contain grains which are predominantly aligned with the Cu lattice and about 10% of 30°-rotated grains (anti-grains). Such graphene films are exclusively monolayer and possess good electrical conductivity, high carrier mobility, and room temperature quantum Hall effect. Magnetoresistance measurements reveal that the reduction of the grain sizes from 150 nm to 50 nm produce increasing Anderson localization and the appearance of a transport gap. Owing to the presence of grain boundaries in these anti-grains, epitaxially grown graphene films possess n-type characteristics and exhibit ultra-high sensitivity to adsorbates.

Introduction

Graphene, a single atomic layer of carbon, has attracted much attention because it allows the condensed-matter physics of an ideal two-dimensional system to be studied on the bench-top [1–3]. There are many methods of preparing graphene, such as micromechanical cleavage from graphite [1, 4], chemical exfoliation methods [5, 6], epitaxial growth on SiC [7, 8], and chemical vapor deposition (CVD) [9–11]. Among these, CVD growth on metals has emerged as the most promising technique for industrial production [12, 13]. During CVD growth of monolayer graphene on metals, individual single-crystalline grains are first formed on the surface, then the growing graphene grains extend across the underlying metal terraces and steps [11, 14–19]. However, most of the grown graphene grains are rotationally misoriented or laterally misaligned, when the grains impinge, graphene grain boundaries (GBs) invariably formed at the interfaces [14–20]. Much effort has been dedicated to producing large-size single crystalline graphene by suppressing nucleation density (a slow method) [15, 17, 21, 22], or growing it from individual grains with the same orientation (a fast method) [23–27]. There have already been some theoretical results concerning the CVD growth mechanisms, including both lateral and vertical heteroepitaxy [28–30]. Lateral growth produce grains which are highly aligned with respect to the metal substrate, with a small percentage of 30°-rotated grains (anti-grains). From the calculated results, lateral heteroepitaxy is favored over vertical growth in graphene growth. However, during CVD growth, high temperatures will induce the copper surfaces to be quasi-liquid [31] and some copper atoms sublime [20, 24–26, 31]. This makes it highly challenging to produce aligned graphene grains on Cu in a consistently reproducible manner. Thermal CVD growths of graphene on Cu usually require temperatures exceeding 1000 °C, which is near Cu's

© 2016 IOP Publishing Ltd

melting point of ~1084 °C. During the growth process, at least 5 nm of Cu will be sublimated from its surface [24–26, 31]. There have been plenty of oriented graphene growth studies recently on single-crystal bulk Cu or films [20, 24–26, 32], but the mechanism of how graphene grains growing laterally and merged seamlessly to form single crystal graphene is not clear.

In the present study, we developed inductively coupled plasma-assisted CVD (ICP-CVD) growth on highly textured (111) and (100) Cu/Ni films at growth temperature lower than 800 °C. A small amount of Ni was alloyed into Cu to reduce Cu sublimation. Using these growth conditions, we observed the lateral heteroepitaxial growth of graphene on Cu, giving rise to highly aligned grains. The graphene grains had two main orientations to the underlying metals: 0° and 30° with ±2.5° deviation. At full coverage, the aligned grains merged seamlessly with only buckled wrinkles and the graphene film possessed high conductivity, high carrier mobility, and quantum Hall effect (QHE) even at room temperature (RT). Owing to the presence of GBs in the coalesced anti-grains, the films also exhibit n-type doping and other interesting properties.

Results and discussion

Lateral heteroepitaxial growth of graphene

Graphene grains and films were grown on smooth single-crystalline Cu/Ni (10:1) films, which were prepared by sputtering Cu/Ni alloy onto *c*-plane sapphire at 300 °C and subsequently annealing it at 800 °C for 10 min. After this treatment, these alloy films exhibited mainly (111) facets with atomic smoothness (figure S1) [25, 32, 33]. ICP-CVD was carried out to attempt the lateral heteroepitaxial growth of graphene. The plasma-assisted process has several advantages over the more commonly used thermal CVD process. Firstly, the plasma-assisted process can be carried out at a substrate temperature lower than 800 °C, which prevents the roughening and sublimation of the catalyst surface. It is worth noting that recently, plasma-assisted CVD has realized the growth of thick graphene films on Ni catalyst [34–36] as well as monolayer graphene film with micron-sized grains on copper foils at temperatures lower than 400 °C [37]. Secondly, the nucleation density can be controlled by adjusting the plasma power, which affects the dissociation of the hydrocarbon feedstock and the concentration of radicals in the gas phase. Moreover, the slight alloying with Ni in the catalyst can effectively reduce the sublimation of Cu and help with surface crystallization (figure S2).

Figures 1(a)–(d) show the atomic force microscope (AFM) height and phase (inset) images of graphene grains recorded at different growth times. The dark regions on the phase images are graphene grains consisting of dendritic lobes. There are no convex hexagonal regions observed across the wafers, and this should be different to the vertical heteroepitaxial growth of graphene on BN [38]. These dendritic lobes are due to the diffusion-limited growth. The phase images, which are sensitive to surfaces of different hardness, viscoelasticity and adhesion [13], clearly showed that most of the graphene grains are hexagons or dendrites composed of hexagons, and most of the hexagonal edges are aligned with the Cu[011¯] steps. The huge densities of the metal steps should provide the initial nuclear sites. The presence of some carbon clusters (marked by green circles), which could act as building blocks for the graphene grains, could be observed on the Cu surface during the initial stage of growth.

To investigate the lattice orientation of the grains, micro-region low-energy electron diffraction (μLEED) was carried out [15, 20, 24, 25] using the same samples as shown in figure 1(d), which showed two main sets of diffraction patterns. The stronger diffraction spots (red) partly overlapped with the diffraction spots of the underlying (111) substrate, indicating epitaxy (red-framed inset image). The weaker one (green) was rotated by approximately ~30°, indicating anti-orientation (green-framed). There was a spread of about 2.5° in each orientation, which originated from the twin structure and the nanoscale roughness of the underlying (111) face [20, 24, 25, 33]. According to previous experimental and theoretical results [20, 24–26, 32, 33], graphene grown on Cu(111) shows preferential alignment to the metal lattice. Anti-grains arise due to edge instability and the presence of 5–7 topological defects. From the comparison of diffraction intensity, ~90% of the grains are aligned (see figure S3).

Raman spectra of the graphene films at different growth stages on alloy substrates are shown in figure 1(h) [39–41]. When individual grains coalesced into a film, the D band associated with edge defects decreased in intensity relative to the G band, along with a blue shift of the G peaks (1595 cm^{-1}–1610 cm^{-1}) and 2D peaks (2690 cm^{-1}–2745 cm^{-1}), indicative of p-type doping effects from the GBs [41, 42]. Interestingly, after the individual grains coalesce into films, their Raman spectra show only low intensity D band, which indicates that at the GB regions, most of the edge defects fuse and reconstruct. The much weaker D band for these coalesced graphene films compared to the nanographene grown previously by catalyst-free methods [43] suggests that the atoms at the GBs in these lateral heteroepitaxial grown graphene films can overcome the activation barrier for reconstruction, i.e., repair of vacancies. Evidence of this can be obtained with scanning tunneling microscopy (STM) and aberration-corrected scanning transmission electron microscopy (TEM) studies, presented in later sections.

It is worth noting that, even when the growth process was interrupted, to be followed by a re-growth, we

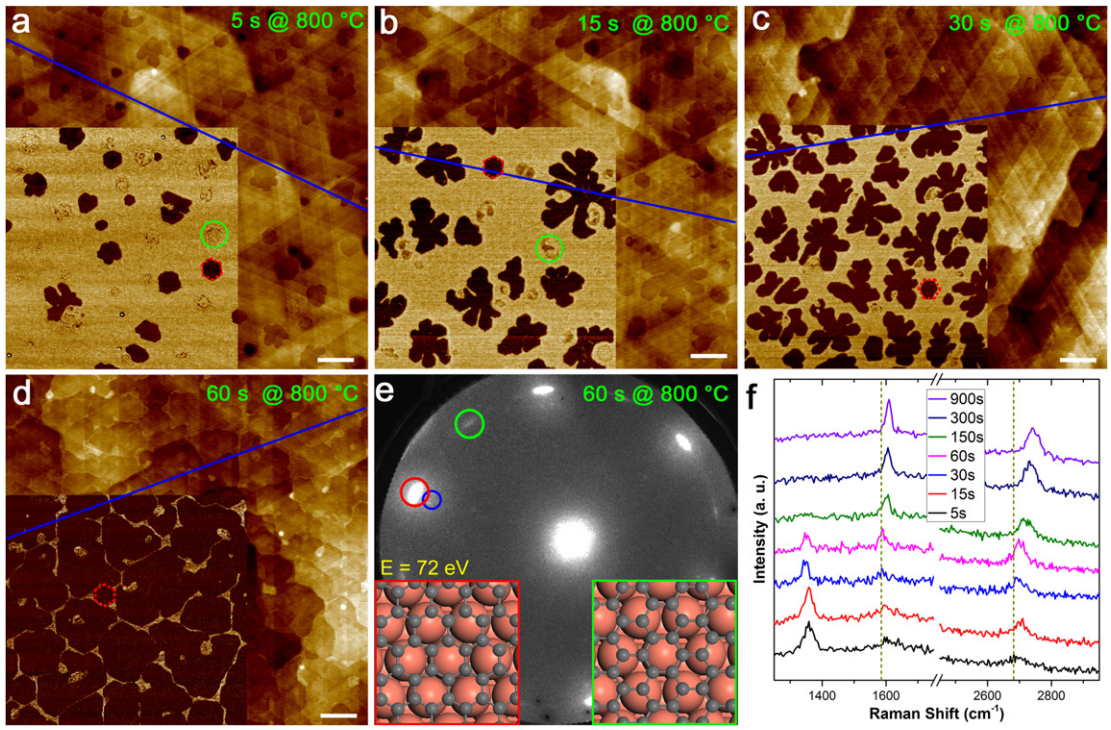


Figure 1. Lateral heteroepitaxy of graphene on highly textured Cu(111) (alloyed with Ni) substrates. Graphene grains at different growth times (a) 5 s; (b) 15 s; (c) 30 s; (d) 60 s are shown. The larger images are AFM height images, and insets are phase images. Typical hexagonal graphene grains are marked by red circles, and graphene clusters are marked by green circles. (e) μLEED pattern of the individual grains, showing two main sets of diffraction patterns (red and green circles) and the diffraction spots of the substrate (blue circle). The inset in red is an illustration of graphene with the same orientation to the underlying (111) facet, and the inset in green is the one with the ~30° rotated anti-grains. (f) Raman spectra of the grown graphene at different growth times on alloy substrates, the defect-related peak nearly disappeared after 150 s of growth. The scale bars in (a)–(d) are all 200 nm.

found that similar results in terms of grain sizes and film quality were obtained as the non-interrupted growth process. This can be explained by the fact that most of the grain grows by lateral epitaxy, i.e. edge expansion due to diffusion of carbon clusters to the edges (figure S4).

Orientation characterization

A lower temperature growth of 750 °C resulted in smaller grain size, but the coalesced films seemed to exhibit good quality (figure S4). To investigate this, the structures of the GBs between orientated grains and anti-grains were analyzed using STM and TEM. Figures 2(a) and (b) shows the typical images in graphene grains, where perfect hexagonal lattices can be observed. The metal covered by graphene still shows the oriented steps. Across the area of 100 nm × 100 nm in figure 2(a), there are no Moiré patterns formed between graphene and underlying Cu(111) surface, which indicates weak interactions between them.

Aberration-corrected scanning TEM was used to analyze the structures of the GBs between orientated and anti-grains [18]. First, micron-sized selected-area electron diffraction (SAED) of the freestanding film (figure 2(c)) confirmed that most of the grains were aligned and only ~10% of them had 30° rotational misalignment, which echoes the results obtained with μLEED. Due to the reactive nature at the GBs [44, 45], residual absorbents remained even after annealing treatments. Atomically resolved details across GB regions and filtered images [18] are shown in figure 2(d). The angle between the two adjacent grains was ~29° and the main dislocations in the GB were meandering lines of alternating pentagons (red) and heptagons (blue) sandwiched by rows of deformed hexagons (green) on each side. These results echo previous TEM studies of CVD graphene films with well-stitched GBs [18], which had a higher growth temperature of 1000 °C [16, 18]. The width of the GB regions was nearly 1 nm, and one can expect that the high density of these GBs will influence the electronic and physical properties of graphene consisting of a patchwork quilt of these GBs.

Growth on Cu(100)

According to theoretical studies of lateral heteroepitaxial growth, the Cu(111) facet is strongly preferred for high quality graphene growth in contrast to Cu(100) [28, 46, 47]. To investigate lateral heteroepitaxial growth on (100)-textured Cu, we sputtered Cu on *a*-plane sapphire and performed CVD growth of graphene. Instead of the hexagonal shaped grains obtained on Cu(111), the graphene grains exhibit

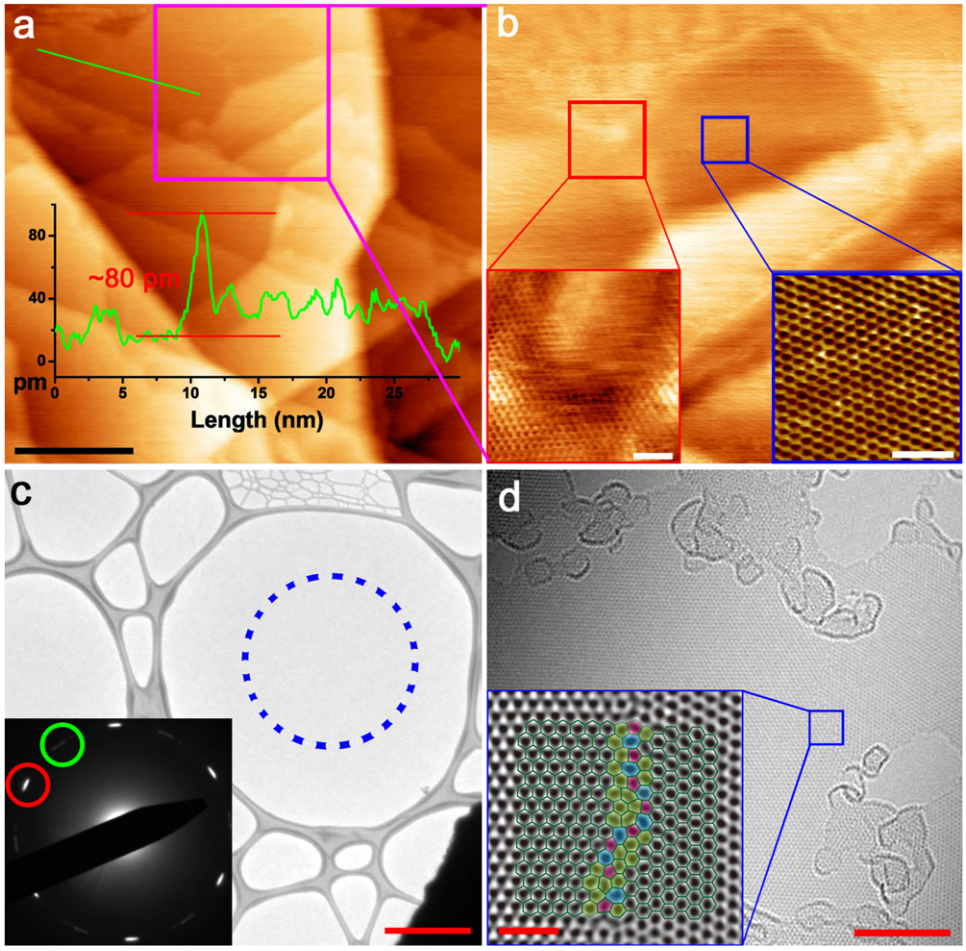


Figure 2. Orientation characterization of lateral heteroepitaxial graphene. (a) and (b) STM images of the partly coalesced graphene film with orientated grains, showing the buckled wrinkles from grain coalescence and seamless stitching with no defective lattice in these regions. (c) TEM images of the coalesced graphene films, the SAED showing two main sets of patterns. (d) Atomic resolution TEM and its local filtered images at the GB region between ~29° misaligned grains, showing a GB with mostly pentagons and heptagons. The scale bars in (a), (c), (d) are 20 nm, 1 μm and 5 nm, in the insets of (b) and (d) are both 1 nm.

rectangular morphology on (100)-textured Cu, as shown in figures 3(a)–(c). At a growth time of 60 s, the coverage of graphene grains reached ~70%, which is similar to the growth coverage of graphene at 40 s on (111) surfaces. The growth rate on (100) facet is at least 1/3 times slower than those on (111) [20, 48], compared in figure 3(d). Due to the four-fold symmetry of the Cu square lattice, the oriented grains here have the equal population to the anti-grains (30° misaligned). After 150 s and 300 s of growth (figures 3(c) and S5), some blank regions without graphene coverage remain. The difficulty in stitching between oriented grains and anti-grains results in a much longer time to grow a continuous film. The lateral heteroepitaxial growths on the (100) facet were also monitored with Raman spectroscopy (figure 3(d)). Even after 900 s of growth time, the defect-related peak (~1350 cm^{-1}) is still present. This can be understood because the superposition of a 6-fold symmetry graphene on a 4-fold symmetry Cu (100) creates many rotational boundaries, which makes it difficult to form a high quality graphene film.

Electrical properties

When the growth time was increased to more than 150 s on the (111)-textured Cu, the individual graphene grains fully cover the surface and coalesce into a continuous film. Figure 4(a) shows a typical optical image of transferred graphene film on SiO_2/Si substrate [15, 49], and insets are photographs of 4 inch graphene on alloy/sapphire and 4 inch transferred graphene on SiO_2/Si wafer. The transferred graphene film shows a highly uniform height of ~1.2 nm over a large area (figure 4(b)). It is worth noting that the graphene films are 100% monolayer. Under the lateral heteroepitaxial growth, carried out in the absence of sublimation, only monolayer graphene grains were formed on the metal surface regardless of the growth temperature or growth time. This robust condition for monolayer graphene will be an important advantage of lateral heteroepitaxy. The Raman spectra of transferred graphene films with different growth times are shown in figure 4(c). The defect-related D bands were reduced with increasing growth time, and the I_D/I_G ratios did not change after coalescence of the grains.

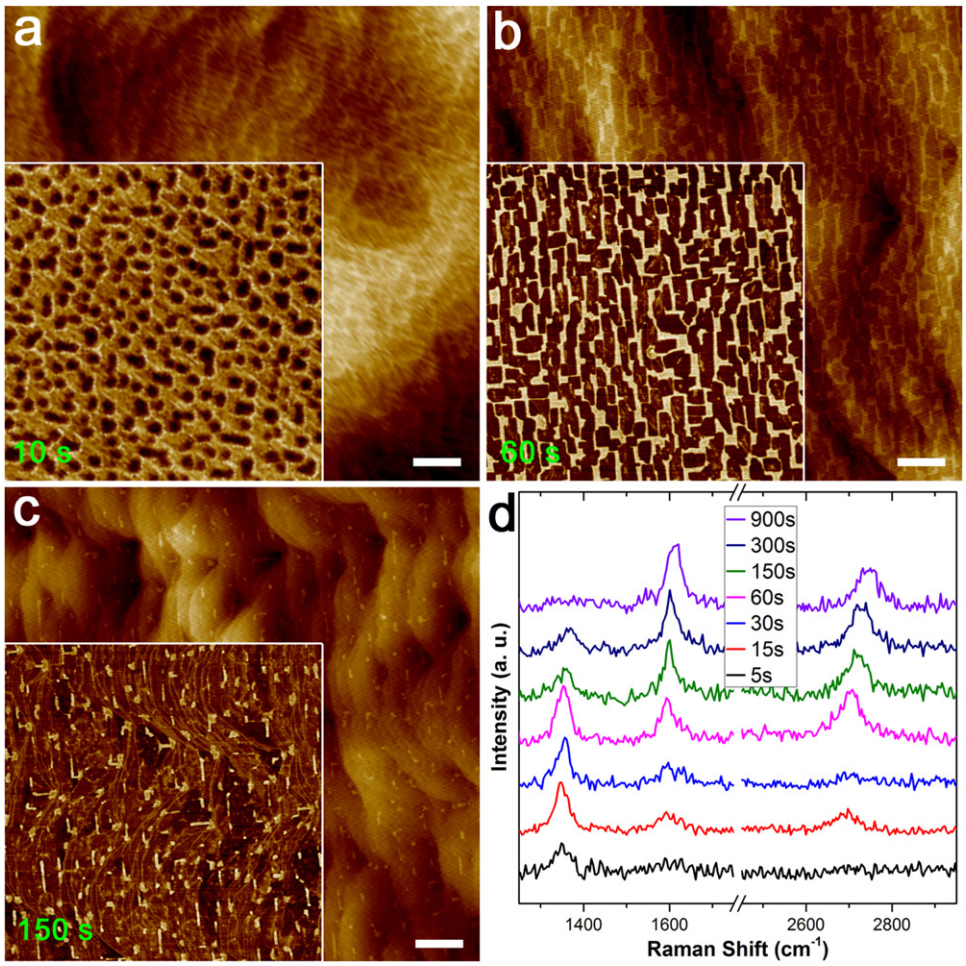


Figure 3. Lateral heteroepitaxial growth of graphene on (100)-textured surfaces. Graphene grains at different growth times: (a) 10 s; (b) 60 s; (c) 150 s. (d) Raman spectra of the grown graphene at different growth times, the defect-related peak is still present after 900 s of growth, and the growth rate is much slower than on (111)-textured films. The scale bars in (a)–(c) are all 200 nm.

The G and 2D bands are blue shifted, similar to the situation before transfer, showing p-type doping caused by ambient exposure [41, 42].

Although most of the nanoscale grains are aligned before fusing, GBs invariably will form due to translational misfit and the presence of anti-grains. These films grown by the fusion of a high density of nanoscale grains resemble a 'mosaic' nanocrystalline graphene, except that the grains in the film are epitaxially aligned to the substrate, thus the coalesced film is able to display certain fingerprints of very high quality graphene such as a sharp Dirac cone when probed by symmetry-dependent spectroscopy. In a recent work, we have shown that mosaic nanocrystalline graphene with a high density of aligned grains with sizes ranging from 50 nm to 150 nm can exhibit robust Dirac cones and phonon dispersion characteristics typical of single crystal graphene, this is despite the fact that the probed area averaged as many as 2.5×10^7 nanoscale grains [50].

To investigate the effects of these GBs on the electronic properties, transferred graphene films on SiO_2/Si substrates were patterned into Hall bar devices of ~1 μm line-width by standard micro/nano fabrications. Dislocations arising from pentagon–heptagon pairs are known to show enhanced reactivity with adsorbates [47, 48] leading to charge transfer to/from GBs. The charge accumulation or depletion due to adsorbates at GB sites will induce the opposite net charge on the surrounding graphene, leading to doping [42], We found that the position of the Dirac point during transport measurements is highly sensitive to the ambient, which is indicative that the film has a high density of GBs. Graphene films exhibited p-type characteristics when exposed to ambient due to the adsorption of moisture on the GBs (figure 4(c)). Annealing in vacuum restores its intrinsic properties, and all of the graphene films with different grain sizes showed *n*-type doping characteristics, which should be attributed to the huge density of GBs undergoing self-doping (i.e., charge-transfer between the GBs and the honeycomb lattices) [42, 51–53]. Field-effect transistor (FET) carrier mobilities of ~3100 $cm^2 V^{-1} s^{-1}$ (800 °C growth) were obtained at RT before annealing, with a neutral point at 17 V (p-doped). After annealing, the neutral point was shifted to −6 V with

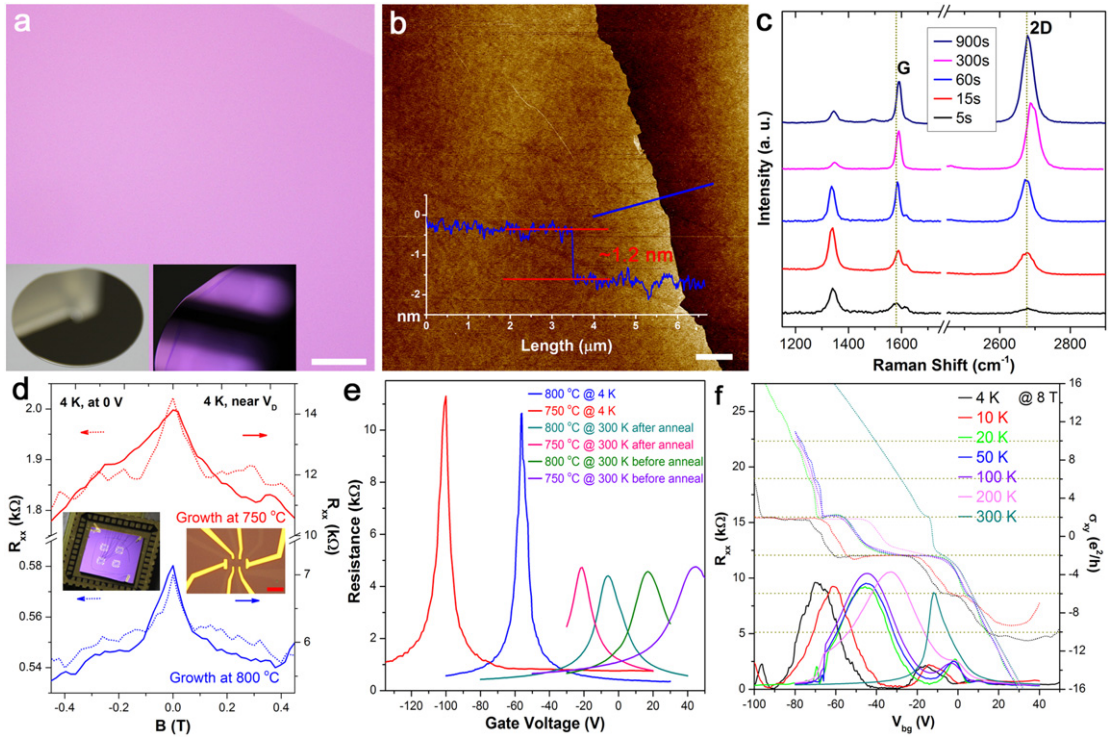


Figure 4. Electronic properties of lateral heteroepitaxial graphene films. (a) Optical image of transferred graphene films on SiO_2/Si wafer, showing 100% monolayer. Insets are photographs of graphene on alloy/sapphire and transferred on SiO_2/Si wafer. (b) AFM image at the torn border, showing that the films are uniform with an average height of ~1.2 nm. (c) Raman spectra of transferred graphene films prepared by different growth times on SiO_2/Si; the D bands were reduced with increasing growth time, before film coalescence. (d) Transport comparison of graphene films at different measurement conditions. (e) Weak localization of different graphene films under a small magnetic field at the gate voltage in the region of the Dirac point and without applying gate voltage. (f) R_{xx} and σ_{xy} of graphene films at different temperatures under a constant magnetic field of 8 T, showing the appearance of QHE even at RT. The scale bar in (a) and (b) is 10 μm and in the inset of (c) is 5 μm.

mobility of ~4900 $cm^2 V^{-1} s^{-1}$. When measured at 4 K in vacuum, the neutral point was shifted to −56 V with higher mobility of ~9100 $cm^2 V^{-1} s^{-1}$. This should be much nearer the intrinsic property of the as-grown graphene where n-type doping by GBs manifests strongly. The same change occurred for the films at 750 °C growth, but with stronger shifts. Their neutral points were first shifted from 44 V (RT before annealing) to −21 V (RT after annealing), and then to −100 V (4 K), with mobilities of 1900–3300 $cm^2 V^{-1} s^{-1}$, and 4900 $cm^2 V^{-1} s^{-1}$, respectively. The graphene films had RT sheet resistances of ~400 Ω/□ (800 °C growth) and ~700 Ω/□ (750 °C growth) at high carrier concentrations.

It has been suggested that GBs are major sources of intervalley scattering, which causes weak localization to manifest as a characteristic form of negative magnetoresistance. To study this we have carried out transport measurements on the graphene films grown on (111)-textured Cu. Figure 4(d) shows the longitudinal resistance (R_{xx}) of the graphene films as a function of the magnetic field at 4 K. When a gate voltage was applied near the Dirac point, the resistance decreased quickly when a small perpendicular magnetic field was applied, resulting in a sharp peak near zero magnetic field, which is characteristic of stronger weak localization or Anderson localization [19, 54, 55]. From Drude conductivity [56], their phase coherence lengths L_ϕ for the graphene films were calculated to be ~125 nm for 800 °C growth and ~82 nm for 750 °C growth, which was similar to their grain sizes before coalescence.

The magneto-transport properties of graphene films were also investigated after film annealing. Figure 4(e) shows the change in R_{xx} and Hall conductivity (σ_{xy}) for graphene films with 800 °C growth as a function of gate voltage under a fixed magnetic field of 8 T at different temperatures (see others in figure S6). All of the data were transformed by tensor inversion [57]. We found that the integer QHE manifests with Landau level filling factors ν of ±2, ±6, and ±10, whereas it manifests with ν of ±2 even at RT [58]. It is well known that GBs will increase the electron localization effect and suppress the QHE [19, 57, 59]. It is therefore surprising that despite the nanoscale grain size and the existence of anti-grains, the graphene films possess the fingerprints of high-quality graphene, such as QHE, good conductivity, and high charge-carrier mobility. Therefore, these results suggest that the presence of a high density of GBs did not degrade the electronic quality of the film significantly; perhaps well-stitched GBs between the highly orientated grains maintain the robust transport properties of graphene typical of Dirac electrons.

Conclusions

In summary, using ICP-CVD methods, monolayer graphene films with predominantly aligned grains have been successfully grown on (111)-textured Cu films at 800 °C in less than 5 min. The temporal evolution of the graphene grains from 5 s (individual grain) to 1 min (near coalescence) during ICP-CVD has been captured using AFM, providing insights into its alignment and fusion. The importance of this work is that it points out that ICP-CVD carried out under high nucleation density condition can produce high quality graphene film in a high throughput manner, thus allowing industrial scalability for large area growth on treated catalyst surfaces. This is a distinct advantage compared to thermal CVD methods using furnaces which typically require significantly longer growth time for large area growth. The coalesced graphene films produced by ICP-CVD are exclusively monolayer, highly uniform, and they also exhibit good electrical conductivity, high carrier mobility, and exhibit QHE at RT despite the presence of a small amount of anti-grains. Due to the presence of GBs and anti-grains, the films exhibit n-type doped characteristics and are endowed with fascinating properties such as ultrahigh sensitivity to adsorbates. Although lateral heteroepitaxial growth also occurs on (100)-textured films, the stitching of GB between the grains is difficult and the film is more defective than film grown on (111)-textured copper.

Methods

Preparation of graphene

The partially or fully covered graphene on metal was grown in a customized Sputter/E-beam/ICP-CVD cluster (base pressure < 1E-6 Torr for ICP-CVD chamber). The typical growth conditions can be described as follows: *c*-plane or *a*-plane sapphire with sputtered Cu/Ni (10:1) film was treated with H_2 plasma at a gas flow rate of 100 sccm and a plasma power of 200 W for 5 min, with the substrate being heated to 750°C–800 °C at 50 mTorr. For the graphene growth, a mixture of H_2 and CH_4 (H_2: CH_4 = 10:1) was introduced into the chamber and the 200 W power plasma was ignited for more than 1 min, with the total pressure maintained at 50 mTorr. After the growth, the graphene film on the alloy metal substrate was cooled to RT under flowing gas, maintained at a constant pressure of 50 mTorr. After growth, the graphene/alloy/sapphire was spin-coated with PMMA (996 K Mw, 4 wt% in ethyl lactate, 2000 rpm for 1 min) to facilitate wet transfer of the graphene film from the Cu/Ni alloy substrate. The etchant used was 0.1 M ammonium persulfate ($(NH_4)_2S_2O_8$) aqueous solution. After two etchings, the PMMA/graphene was cleaned in DI water. Finally, the graphene was transferred onto SiO_2/Si wafers for transport studies after the PMMA was removed with acetone. In addition, annealing at 400 °C for more than 30 min was needed to further reduce the doping effect from water and PMMA.

Characterizations

The graphene films transferred on TEM grids were observed by TEM (FEI Titan 80-300 probe aberration-corrected scanning TEM with monochromator, operated at 60 kV). The freshly grown graphene on alloy/sapphire was also characterized with UHV-STM (Omicron). Before the measurements, all of the samples were annealed in UHV at ~250 °C for 12 h to remove the surface adsorbates and contaminants. The crystalline structure of the fresh graphene on alloy/sapphire was also characterized by μLEED (selected area ~5 μm) in an Elmitec LEEM III system (UHV, base pressure $<10^{-10}$ Torr), and the applied starting voltage was <100 V.

Device fabrications and electrical measurements

The graphene films transferred onto SiO_2/Si wafers were fabricated into FET devices for physical property measurements. All of the electrical contacts in the devices (Cr/Au, 5 nm/80 nm, thermal evaporated) with graphene films were patterned by e-beam lithography (Nova NanoSEM 230). Ar plasma etching (10 mTorr, 50 W, 20 s) was used for etching the graphene. Standard lift-off processes were performed for the final devices. After the devices' fabrications, the graphene films were measured under vacuum (~10 Torr) in a physical property-measurement system (Quantum Design EverCool II). All of the resistance levels used in the main content were measured using low-frequency lock-in detection (SR 830) with a driving current of 5–50 nA.

Acknowledgments

This work is supported by NRF 2014 NRF-POC-001 grant 'Industrially Scalable Approach for Growth and Transfer of Large Area Graphene' as well as funding by NRF under the Medium-sized Centre grant. LG is also supported by the Fundamental Research Funds for the Central Universities (0204-1438-0004).

References

[1] Novoselov K S, Geim A K, Morozov S V, Jiang D, Zhang Y, Dubonos S V, Grigorieva I V and Firsov A A 2004 *Science* **306** 666
[2] Geim A K 2009 *Science* **324** 1530
[3] Novoselov K S, Fal'ko V I, Colombo L, Gellert P R, Schwab M G and Kim K 2012 *Nature* **490** 192
[4] Novoselov K S, Jiang D, Schedin F, Booth T J, Khotkevich V V, Morozov S V and Geim A K 2005 *Proc. Natl Acad. Sci. USA* **102** 10451
[5] Stankovich S, Piner R D, Nguyen S T and Ruoff R S 2006 *Carbon* **44** 3342
[6] Stankovich S, Dikin D A, Dommett G H B, Kohlhaas K M, Zimney E J, Stach E A, Piner R D, Nguyen S T and Ruoff R S 2006 *Nature* **442** 282

[7] Berger C *et al* 2004 *J. Phys. Chem.* B **108** 19912
[8] Berger C *et al* 2006 *Science* **312** 1191
[9] Reina A, Jia X T, Ho J, Nezich D, Son H B, Bulovic V, Dresselhaus M S and Kong J 2009 *Nano Lett.* **9** 30
[10] Kim K S *et al* 2009 *Nature* **457** 706
[11] Li X S *et al* 2009 *Science* **324** 1312
[12] Bae S K *et al* 2010 *Nat. Nanotechnol.* **5** 574
[13] Gao L B, Ni G X, Liu Y P, Liu B, Neto A H C and Loh K P 2014 *Nature* **505** 190
[14] Duong D L *et al* 2012 *Nature* **490** 235
[15] Gao L B *et al* 2012 *Nat. Commun.* **3** 699
[16] Tsen A W *et al* 2012 *Science* **336** 1143
[17] Li X S, Magnuson C W, Venugopal A, Tromp R M, Hannon J B, Vogel E M, Colombo L and Ruoff R S 2011 *J. Am. Chem. Soc.* **133** 2816
[18] Huang P Y *et al* 2011 *Nature* **469** 389
[19] Yu Q K *et al* 2011 *Nat. Mater.* **10** 443
[20] Nie S, Wofford J M, Bartelt N C, Dubon O D and McCarty K F 2011 *Phys. Rev.* B **84** 155425
[21] Hao Y F *et al* 2013 *Science* **342** 720
[22] Yan Z *et al* 2012 *ACS Nano* **6** 9110
[23] Lee J H *et al* 2014 *Science* **344** 286
[24] Robinson Z R, Tyagi P, Mowll T R, Ventrice C A and Hannon J B 2012 *Phys. Rev.* B **86** 235413
[25] Ago H *et al* 2015 *Chem. Mater.* **27** 5377
[26] Nguyen V L *et al* 2015 *Adv. Mater.* **27** 1376
[27] Sutter P W, Flege J I and Sutter E A 2008 *Nat. Mater.* **7** 406
[28] Yuan Q H, Yakobson B I and Ding F 2014 *J. Phys. Chem. Lett.* **5** 3093
[29] Zhang X Y, Li H and Ding F 2014 *Adv. Mater.* **26** 5488
[30] Shu H B, Chen X S, Tao X M and Ding F 2012 *ACS Nano* **6** 3243
[31] Wang Z J *et al* 2015 *ACS Nano* **9** 1506
[32] Hu B S *et al* 2012 *Carbon* **50** 57
[33] Reddy K M, Gledhill A D, Chen C H, Drexler J M and Padture N P 2011 *Appl. Phys. Lett.* **98** 113117
[34] Volotskova O, Levchenko I, Shashurin A, Raitses Y, Ostrikov K and Keidar M 2010 *Nanoscale* **2** 2281
[35] Levchenko I, Volotskova O, Shashurin A, Raitses Y, Ostrikov K and Keidar M 2010 *Carbon* **48** 4570
[36] Qi J L, Zheng W T, Zheng X H, Wang X and Tian H W 2011 *Appl. Surf. Sci.* **257** 6531
[37] Boyd D A *et al* 2015 *Nat. Commun.* **6** 6620
[38] Yang W *et al* 2013 *Nat. Mater.* **12** 792
[39] Ferrari A C *et al* 2006 *Phys. Rev. Lett.* **97** 187401
[40] Das A *et al* 2008 *Nat. Nanotechnol.* **3** 210
[41] Bruna M, Ott A K, Ijas M, Yoon D, Sassi U and Ferrari A C 2014 *ACS Nano* **8** 7432
[42] Ren J C, Ding Z J, Zhang R Q and Van Hove M A 2015 *Phys. Rev.* B **91** 045425
[43] Zhang L C, Shi Z W, Liu D H, Yang R, Shi D X and Zhang G Y 2012 *Nano Res.* **5** 258
[44] Feng X F, Maier S and Salmeron M 2012 *J. Am. Chem. Soc.* **134** 5662
[45] Yasaei P *et al* 2014 *Nat. Commun.* **5** 4911
[46] Ogawa Y, Hu B S, Orofeo C M, Tsuji M, Ikeda K, Mizuno S, Hibino H and Ago H 2012 *J. Phys. Chem. Lett.* **3** 219
[47] Jacobberger R M and Arnold M S 2013 *Chem. Mater.* **25** 871
[48] Wood J D, Schmucker S W, Lyons A S, Pop E and Lyding J W 2011 *Nano Lett.* **11** 4547
[49] Reina A, Son H B, Jiao L Y, Fan B, Dresselhaus M S, Liu Z F and Kong J 2008 *J. Phys. Chem.* C **112** 17741
[50] Nai C T, Xu H, Tan S J R and Loh K P 2016 *ACS Nano* **10** 1681
[51] Tapaszto L, Nemes-Incze P, Dobrik G, Yoo K J, Hwang C and Biro L P 2012 *Appl. Phys. Lett.* **100** 053114
[52] Peres N M R, Guinea F and Neto A H C 2006 *Phys. Rev.* B **73** 125411
[53] Koepke J C, Wood J D, Estrada D, Ong Z Y, He K T, Pop E and Lyding J W 2013 *ACS Nano* **7** 75
[54] Moser J, Tao H, Roche S, Alzina F, Torres C M S and Bachtold A 2010 *Phys. Rev.* B **81** 205445
[55] Abrahams E, Anderson P W, Licciardello D C and Ramakrishnan T V 1979 *Phys. Rev. Lett.* **42** 673
[56] McCann E, Kechedzhi K, Fal'ko V I, Suzuura H, Ando T and Altshuler B L 2006 *Phys. Rev. Lett.* **97** 146805
[57] Lafont F *et al* 2014 *Phys. Rev.* B **90** 115422
[58] Novoselov K S *et al* 2007 *Science* **315** 1379
[59] Cummings A W, Cresti A and Roche S 2014 *Phys. Rev.* B **90** 161401